Ocean Engineering 258 (2022) 111733

Contents lists available at ScienceDirect

Ocean Engineering

journal homepage: www.elsevier.com/locate/oceaneng

CFD analysis of the effect of heterogeneous hull roughness on ship resistance

Roberto Ravenna [a,*], Soonseok Song [b], Weichao Shi [a], Tonio Sant [c], Claire De Marco Muscat-Fenech [c], Tahsin Tezdogan [a], Yigit Kemal Demirel [a]

[a] Department of Naval Architecture, Ocean and Marine Engineering, Faculty of Engineering, University of Strathclyde, 100 Montrose Street, G4 0LZ, Glasgow, UK
[b] Department of Naval Architecture & Ocean Engineering, College of Engineering, Inha University, 100 Inha-ro, Incheon, 22212, South Korea
[c] Department of Mechanical Engineering, Faculty of Engineering, University of Malta, Msida, MSD2080, Malta

ARTICLE INFO

Keywords:
Roughness effect
Computational fluid dynamics (CFD)
Heterogeneous roughness
Ship resistance
KRISO Container ship (KCS)

ABSTRACT

Hull roughness significantly increases ship resistance, power, and fuel consumption. Although it is typically spatially heterogeneous, little research has dealt with heterogeneously distributed roughness on ship hulls. Therefore, this study investigates the heterogeneous hull roughness effect on ship resistance using Computational Fluid Dynamics (CFD). A series of CFD simulations were conducted on the KRISO Container Ship (KSC) hull model to accurately predict the effect of heterogeneous hull roughness on ship resistance. Specifically, the StarCCM + software package was adopted to develop Unsteady Reynolds Averaged Navier–Stokes (URANS)-based CFD simulations with a modified wall-function approach. Various surface coverage conditions were modelled, including homogeneous (i.e., smooth and full rough conditions) and heterogeneous conditions (i.e., different smooth/rough wetted surface ratios). Eventually, the present findings showed that increased roughness on the bulbous bow region has the most significant impact on ship resistance. Moreover, the introduction of a so-called roughness impact factor correlated the added resistance of the heterogeneous roughness scenarios to the corresponding rough wetted surface area. Accordingly, the rough bulbous bow scenario presented a higher roughness impact factor than the other rough hull cases.

1. Introduction

Naval architects, shipowners, and operators are fully aware of the economic and environmental penalties linked to a poorly maintained hull. It is well established that hull roughness is foremost responsible for the decay of ship performance over time. According to (Townsin, 2003; Tezdogan and Demirel, 2014), biofouling accumulation, antifouling coating failure, and corrosion are the leading causes of the increase of roughness on the hull surfaces. Nevertheless, our understanding of the hull roughness effect on ship resistance is limited to date. Dry-dock and fouling control coating (FCC) strategies to mitigate the roughness effect on ship resistance are arguably incomplete. The typical approach of ignoring the vessel's underwater hull conditions for long dry-dock intervals is a major cause of considerable losses to a fleet's economy. Furthermore, roughness accumulates in a complicated and typically heterogeneous way on ship hulls resulting in more difficult predictions of its effects on ship resistance. Therefore, extending the knowledge on hull roughness effects on ship resistance is essential, especially from a biofouling management perspective. Hence, it is essential to conduct further study into the correlation between roughness and drag to develop accurate CFD prediction methods and, ultimately, hull maintenance strategies.

Surface roughness leads to increased turbulence manifesting itself as turbulent shear stress and wall shear stress increase. Ultimately the velocity, U^+, in the turbulent boundary layer decreases (Fig. 1). The mean log-law velocity profile decrease within the boundary layer is called the roughness function, ΔU^+, and it is a unique characteristic of a surface covered with a specific roughness. Different studies, such as (Haslbeck, 1992), documented the effects of coatings and biofouling on ship powering through full-scale trials. Schultz validated the assumption that roughness functions can accurately represent given hull surface conditions by comparing his experimental results with others (Schultz, 2004b). Researches such as (Candries, 2001; Schultz, 2002, 2004a, 2007; Shapiro, 2004; Schultz and Flack, 2005; Flack and Schultz, 2010; Demirel, 2017a), have widely adopted Granville's similarity law scaling procedure (Granville, 1958, 1978) to predict the effect of hull roughness

* Corresponding author.
E-mail address: roberto.ravenna@strath.ac.uk (R. Ravenna).

https://doi.org/10.1016/j.oceaneng.2022.111733
Received 3 February 2022; Received in revised form 29 April 2022; Accepted 10 June 2022
Available online 2 July 2022

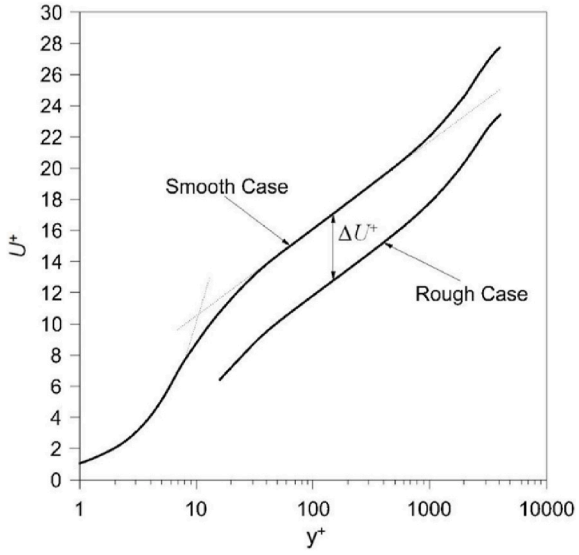

Fig. 1. The roughness effect on a log-law velocity profile, adapted from (Schultz and Swain, 2000).

on ship resistance, due to its robustness and cost-effectiveness, as pointed out by (Oliveira et al., 2018). In other words, roughness functions can accurately represent given hull surface conditions. Hence, theoretical and numerical methods based on the turbulent boundary layer theory can accurately predict the roughness effect on ship resistance, provided that the roughness function of the surface is known (Demirel, 2015).

However, Granville's theoretical method is limited by several simplifications. The Computational Fluid Dynamics (CFD) approach is a valid alternative to Granville's method as it avoids the non-linear problems of theoretical studies and dynamically computes the roughness function for each discretised cell (Stern et al., 2015) and, as suggested by (Atlar et al., 2018), it is cost-efficient compared to experimental approaches and can overcome related shortcomings. In fact, the assumption of a constant roughness function along the flat plate may lead to scaling problems and inaccurate added resistance predictions, as underlined by (Demirel et al., 2017a). Furthermore, the 2D flat plate assumption neglects the 3D effect, as criticised by (Atlar et al., 2018). According to (Demirel et al., 2017b; Atlar et al., 2018; Song et al., 2019, 2020a), the ship resistance predictions are more accurate in CFD since the 3D effect of the hull is considered, and the ship can be modelled in full-scale. It should be noted that these studies also recommended further investigations into the effect of hull roughness on ship resistance to characterise all possible real-life conditions in terms of surface roughness. Accordingly, an increasing number of studies adopted the CFD approach for investigating the roughness effect on ship resistance. Until recently, regardless of the inherently heterogeneous hull roughness distribution of in-service ships, most studies dealing with hull roughness assume that the hull roughness is homogeneous (Farkas et al., 2018; Demirel et al., 2019; Song et al., 2020a).

The effects of heterogeneous distribution of roughness and the benefits of partial hull cleaning were first investigated by dividing the hull into different sections (Vargas et al., 2019). They conducted CFD simulations on a surface combatant exposed to different roughness scenarios. The findings indicated that the increase in the skin friction resulting from localised roughness is highest at the bow, followed by sides, flat bottom, stern, and transom. In (Östman et al., 2019) the authors carried out a CFD analysis investigating the potential of a selective application of different quality coatings on a full-scale tanker. The regions with concentrated high skin friction were modelled with a high-quality coating (low roughness), while the rest of the hull was modelled with a low-quality coating. The results confirmed the expectations: this selective approach can reduce the ship resistance compared to when the inferior coating is applied to the entire hull.

Furthermore, in (Song et al., 2021c, 2021d) the heterogeneous hull roughness effect on ship hydrodynamics through experimental fluid dynamics (EFD) and CFD was investigated. In our previous study, (Song et al., 2021c), the Wigley hull was modelled with different hull roughness conditions by applying sand-grit on the hull surface in various configurations (i.e., smooth and full-rough, ¼-bow-rough, ¼-aft-rough, ½-bow-rough and ½-aft-rough). The increased roughness in the forward wetted surface of the Wigley hull caused more added resistance than the hull roughness in its other parts. Hence, the findings suggest the possibility of prioritising a partial hull cleaning depending on the impact of the roughness in different hull regions. In (Song et al., 2021), CFD simulations were performed using the modified wall-function approach and the roughness function model of (Song et al., 2020c). In their study, the CFD model was validated to predict the effect of roughness on ship resistance for 3D hulls. The findings showed good agreement between the CFD modified wall-function approach, Granville's similarity law, and measurements from a ship model towing tests with a rough surface (Song et al., 2021b).

A recently published paper dealt with many of the issues of heterogeneous hull roughness on the benchmark tanker KVLCC2, (Kim et al., 2022). Their study included self-propulsion simulations with SHIP-FLOW, a code developed by FLOWTECH, on the induced relation between hull surface roughness and ship performance. They estimated the attainable reduction of propulsion power by hull surface treatment as a cleaning efficiency index (CEI), which is defined as the ratio between the delivered horsepower reduction per unit cleaning area. Similarly to the roughness impact factor (RIF) that will be introduced later in the present study (Results section), the CEI number recommends partial hull treatment based on cost-benefit analysis. Furthermore, the study showed the economic viability of partial hull treatment. However, only the heterogeneous roughness effect on the KVLCC2 hull was investigated. Different ship types should be investigated to understand the optimum hull surface maintenance strategy better.

The promising findings of the few studies addressing the effect of heterogeneous distribution of hull roughness are limited to the ship types considered (the Wigley hull, a tanker, and a surface combatant). Despite these recent studies, our understanding of the effect of heterogeneous hull roughness is still limited. The different impacts of hull roughness on different hull regions need to be investigated for better comprehension. The present study aims to fill this research gap by investigating the effect of heterogeneous roughness on the hydrodynamic resistance of the well-known Kriso Container Ship (KCS) hull using CFD, also supporting a targeted strategy for hull maintenance. Furthermore, the CFD simulations in this study will provide accurate data to assess how the heterogeneous hull roughness affects the flow regime around the hull.

The present study is a CFD investigation conducted on the benchmark KCS hull in heterogeneous hull roughness conditions, (Fig. 2). Unsteady Reynolds Averaged Navier–Stokes (URANS)-based CFD simulations with a modified wall-function approach were developed in StarCCM+. The scenarios modelled include homogeneous (i.e., smooth and full rough conditions) and heterogeneous conditions (i.e., different smooth/rough wetted surface ratios). A so-called *Roughness Impact Factor, RIF,* was introduced to correlate the added resistance of the heterogeneous roughness scenarios to the corresponding rough wetted surface area. The paper is structured as follows:

- Section 2 presents the methodology adopted, including the numerical modelling. Details of the modified wall-function approach, mathematical formulations, geometry and boundary conditions, and mesh generations are given in this section.
- Section 3 discusses the results of the current CFD investigation. The effects of heterogeneous hull roughness on the hydrodynamics of the ship were assessed and discussed in this section. Moreover, the

Fig. 2. KCS hull split by patch for creating heterogeneous roughness scenarios.

dimensionless *roughness impact factor* correlated the various hull roughness conditions with the predicted resistance coefficients. Finally, roughness Reynolds number values and boundary layer distributions of the heterogeneous configurations were compared with the homogeneous full rough and full smooth cases.

- Section 4 gives the conclusions of the present study. In this section, the results are further summarised and discussed, along with recommendations for future studies.

2. Methodology

2.1. Approach

Fig. 3 shows a schematic illustration of the CFD methodology adopted to investigate the effect of heterogeneous distributions of hull roughness on the well-known KRISO Container Ship (KCS) (KCS Geometry and Conditions, 2008). The model-scale numerical towing tests investigated the impact of various heterogeneous hull roughness conditions (different smooth/rough wetted surface coverage ratios) and effects on ship resistance. These roughness scenarios were designed to investigate the potential of low-cost targeted hull maintenance.

The simulations were developed in the StarCCM + software package (Version 15.06.007-R8), adopting the Unsteady Reynolds Averaged Navier–Stokes (URANS)-based CFD with the modified wall-function model recently validated in (Song et al., 2020d). The skin friction coefficient, C_f, roughness Reynolds number, k^+, and boundary layer on the hull surfaces were examined and correlated with the findings. The report figures for these parameters in Section 3 will support a better comprehension of the impact of the increased roughness of different hull conditions on ship resistance.

Currently, the physical modelling of the roughness sources in CFD, such as coatings or biofouling is practically impossible due to their

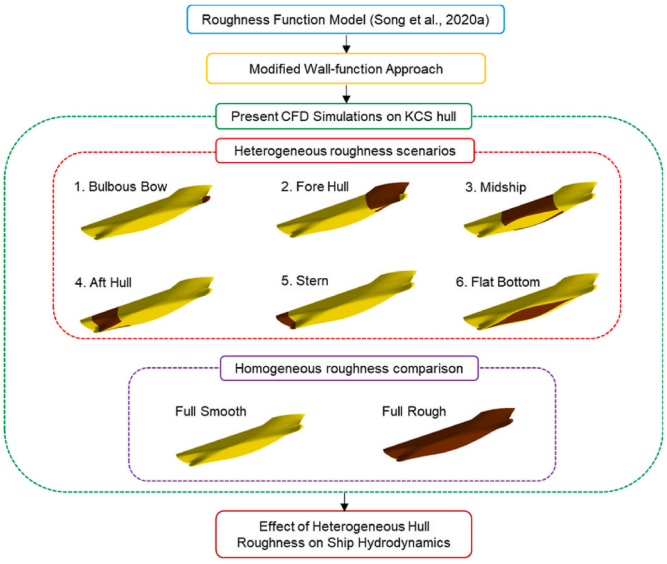

Fig. 3. Schematic illustration of the methodology adopted. The rough areas of the tested scenarios are denoted in brown, and the smooth ones are in yellow.

complex geometries. However, as said in the Introduction, once the roughness function model is known, it can be employed in the wall-function or the turbulence models of the CFD simulations. It is of note that the velocity U^+ in the turbulent boundary layer is not uniform on the rough surface due to differences in the friction velocity distribution. The effect of U^+ varying along the surface can be simulated using CFD-based models as the friction velocity is dynamically computed for each discretised cell. CFD-based URANS are essential to simulate the surface roughness phenomenon by means of a fully non-linear method. The URANS solution is time accurate as it is based on the Implicit Unsteady approach. In the Implicit Unsteady method, each physical time-step involves some number of inner iterations to converge the solution for that given instant of time. Therefore, the resulting frictional resistance can be more accurately computed using URANS CFD methods.

2.2. Numerical modelling

2.2.1. Mathematical formulations

The governing equations of this hydrodynamics study are given in tensor notation and Cartesian coordinates by equations (1) and (2), (Ferziger et al., 2020):

$$\frac{\partial(\rho\overline{u}_i)}{\partial x_i} = 0 \tag{1}$$

$$\frac{\partial(\rho\overline{u}_i)}{\partial t} + \frac{\partial}{\partial x_j}\left(\rho\overline{u}_i\overline{u}_j + \rho\overline{u_i'u_j'}\right) = -\frac{\partial\overline{p}}{\partial x_i} + \frac{\partial\overline{\tau}_{ij}}{\partial x_j} \tag{2}$$

where, ρ is the density, $\overline{u}_i$ is the averaged velocity vector, $\rho\overline{u_i'u_j'}$ is the Reynolds stress, $\overline{p}$ is the averaged pressure, $\overline{\tau}_{ij}$ is the mean viscous stress tensor components. Newtonian fluid's viscous stress can be expressed as in equation (3):

$$\overline{\tau}_{ij} = \mu\left(\frac{\partial\overline{u}_i}{\partial x_j} + \frac{\partial\overline{u}_j}{\partial x_i}\right) \tag{3}$$

where, μ is the dynamic viscosity. The Reynolds stress can be written as in equation (4), using the Boussinesq hypothesis:

$$-\rho\overline{u_i'u_j'} = \mu_t\left(\frac{\partial\overline{u}_i}{\partial x_j} + \frac{\partial\overline{u}_j}{\partial x_i}\right) - \frac{2}{3}\left(\rho k + \mu_t\frac{\partial\overline{u}_k}{\partial x_k}\right)\delta_{ij} \tag{4}$$

where, μ_t is the turbulent eddy viscosity, k is turbulent kinetic energy, and δ_{ij} is the Kronecker delta.

The commercial CFD software STAR-CCM + using URANS and finite volume methods, solved the above-average continuity and momentum equations for incompressible flows. The CFD solver used a second-order upwind convection scheme and a first-order temporal discretisation for the momentum equations. On the other hand, the continuity equations were solved in a segregated manner and linked to the momentum equations with a predictor-corrector algorithm. The k-ω SST (Shear Stress Transport) turbulence model (Menter, 1994) was used with a second-order convection scheme. This turbulent model combines k-ω and k-ε formulations for an accurate near wall treatment of the effects of turbulence, and an overall enhanced prediction of adverse pressure gradients and separating flow. Although the effect of hull roughness on frictional resistance is dominant compared to other resistance

components, recent studies claim that its effect on other resistance components is still essential for accurate prediction of the ship resistance (Oliveira et al., 2018; Farkas et al., 2020; Song et al., 2020b). The Volume of Fluid (VOF) model with Eulerian multiphase was used to simulate surface gravity waves on the interface between air and water. The VOF model allows specifying wave initial and boundary conditions, and as in this study, the ship is towed through calm water, a flat VOF wave was defined. In other words, the VOF model guarantees more accurate predictions of the effect of hull roughness on ship resistance. Furthermore, the free surface water level changes over time during the simulation. Hence, it is of note that the free surface effects were modelled using High-Resolution Interface Capturing (HRIC).

2.2.2. Modified wall-function approach

An increase in surface roughness reduces the boundary layer thickness and causes an increase in flow turbulence. Hence, the turbulent stress, wall shear stress and ultimately the skin friction increase. The roughness effect can also be seen as a downward shift of the non-dimensional velocity profile in the turbulent boundary layer log-law region. The non-dimensional velocity profile (U^+) in the log-law region for a rough surface can be written as equation (5):

$$U^+ = \frac{1}{\kappa}\ln y^+ + B - \Delta U^+ \tag{5}$$

where κ is the von-Karman constant, y^+ is the non-dimensional normal distance from the boundary ($y^+ = yU_\tau/\nu$), B is the smooth wall log-law intercept. The downward shift of the non-dimensional velocity profile (ΔU^+), also known as "roughness function", is a unique characteristic of a rough surface. In other words, different rough surfaces are characterised by different roughness functions to be modelled experimentally (Granville, 1958). Then, once the experimental roughness function model of the surface is developed, it can then be implemented in the wall function of the CFD model.

The roughness function, ΔU^+ is a function of the roughness Reynolds number, k^+, which is defined as equation (6):

$$k^+ = \frac{kU_\tau}{\nu} \tag{6}$$

where the roughness length scale of the surface, k, is normalised and termed the roughness Reynolds number, k^+, given by equation (6) in which U_τ is the velocity based on wall shear stress defined as equation (7):

$$U_\tau = \sqrt{\tau_w/\rho} \tag{7}$$

where τ_w is the wall shear stress and ρ is the water density.

The selection of the roughness length scale, k, is critical to defining a roughness function model. However, k only affects the abscissa of the profile of roughness functions against roughness Reynolds numbers. For this reason, k can be selected such that the ΔU^+ values fall on a predefined roughness function model (Demirel, 2015). In other words, the roughness Reynolds numbers, k^+, and roughness length scale, k, can be used to develop a roughness function model to represent the coating or fouling conditions examined. Typically, k is defined as a multiple of Rt_{50} as in the present model, where Rt_{50} is the maximum peak to trough roughness height measured over a 50 mm interval; Rt_{50} is also termed the Average Hull Roughness (AHR).

Equation (8) shows the roughness function model employed in this study using STAR-CCM+'s built-in roughness function model (Song et al., 2020b). developed the model in Fig. 4 from the towing tests of a flat plate covered with sand (aluminium oxide, 60/80 grit) (Song et al., 2021b). The hull surface conditions represented are a medium rough case ($Rt_{50} = 353$ μm) as of a medium developed slime (Schultz, 2004b).

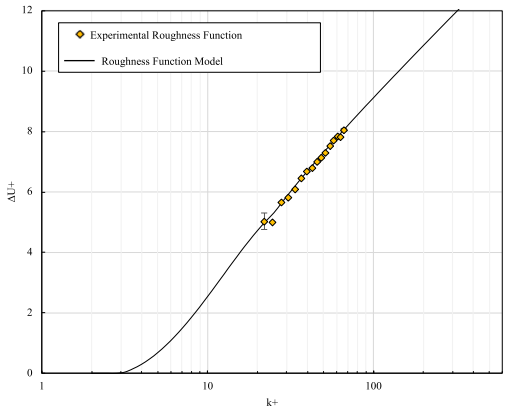

Fig. 4. Experimental roughness function model and roughness function model adopted (Song et al., 2020b; Song et al., 2021b).

$$\Delta U^+ = \begin{cases} 0 & \rightarrow \quad k^+ < 3 \\ \frac{1}{\kappa}\ln\left[0.49k^+ - 3\left(\frac{k^+-3}{25-3}\right)\right]^{\sin\left[\frac{\pi}{2}\frac{\log(k^+/3)}{\log(25/3)}\right]} & \rightarrow \quad 3 \le k^+ < 25 \\ \frac{1}{\kappa}\ln(0.49k^+ - 3) & \rightarrow \quad 25 \le k^+ \end{cases} \tag{8}$$

In which κ is the von-Karman constant ($\kappa = 0.42$).

2.2.3. Geometry and boundary conditions

The CFD simulations were carried out on the well-known container ship KCS modelled on the scale factor of 75. Table 1 presents the particulars of the full-scale and model KCS adapted from (Kim et al., 2001) and (Larsson et al., 2013). Table 2 and Fig. 5 depict the characteristics of the different hull roughness scenarios of the CFD simulations. It is noted that the difference between the geometry of the hull in the present study (without rudder) and in the literature (with rudder) (Song et al., 2020b) does not compromise the validity of the CFD modified-wall function approach used as shown in Section 2.3.2. Furthermore, the results of the present CFD simulations were calculated using the same the WSA of the KCS model given in the literature ($WSA_{Total} = 1.6753\,m^2$). Using a universally adopted WSA for the calculations guarantees more straightforward comparisons across different studies on the KCS hull.

Fig. 6 shows the computational domain, a towing tank with the size chosen following the International Towing Tank Committee (ITTC) recommendations (ITTC, 2011) and similar studies (Song et al., 2020b; 2021a; 2021c; Terziev et al., 2020). A pressure outlet was selected for the outlet boundary condition, while a velocity inlet was applied for all the other surfaces of the domain (inlet, sidewalls, bottom and top). These boundary conditions simulated the deep water and infinite air

Table 1
KRISO Container Ship (KCS) Full-scale and Model-scale principal characteristics.

Parameters		Full-scale	Model-scale
Scale factor	λ	1	75
Length between the perpendiculars	L_{PP} (m)	230	3.0667
Length of waterline	L_{WL} (m)	232.5	3.1
Beam at waterline	B_{WL} (m)	32.2	0.4293
Depth	D (m)	19.0	0.2533
Design draft	T (m)	10.8	0.144
Wetted surface area w/o rudder	WSA_{Total} (m^2)	9424	1.6753
Displacement	∇ (m^3)	52030	693.733
Block coefficient	C_B	0.6505	0.6505
Design speed	V $(kn,\ m/s)$	24	1.426
Froude number	F_n	0.26	0.26
Reynolds number	R_n	$2.4{\cdot}10^9$	$3.7{\cdot}10^6$
Centre of gravity	KG (m)	7.28	0.0971
Metacentric height	GM (m)	0.6	0.008

Table 2
Test scenarios of the KCS model simulations in heterogeneous hull roughness conditions.

Roughness scenario	% Rough wetted surface area % WSA_{Rough} (%)
1. Bulbous Bow	2.57
2. Fore Hull	17.68
3. Midship	29.50
4. Aft Hull	19.13
5. Stern	8.14
6. Flat Bottom	22.92
Full Rough	100

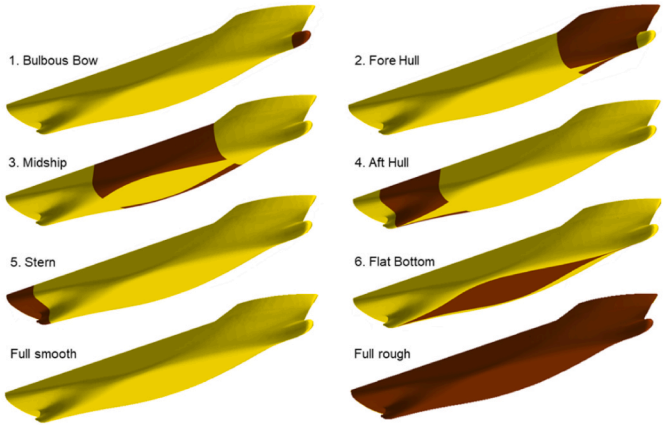

Fig. 5. Test scenarios of the KCS model simulations in heterogeneous hull roughness conditions.

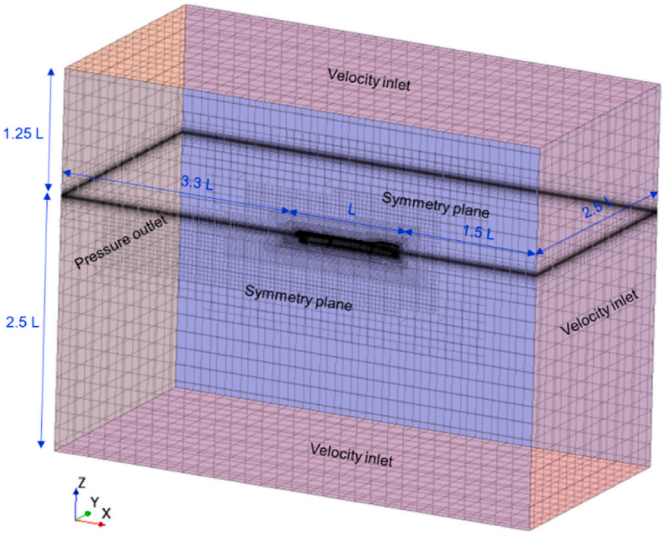

Fig. 6. Computational domain and boundary conditions of the KCS model simulations.

conditions. The tank's bottom, top and sidewalls were selected as slip-walls, whilst for free-surface modelling, the no-slip wall type boundary condition was used on the hull surfaces. The symmetry boundary condition was applied on the vertical centre plane of the domain to shorten the computational time. The model ship was free to sink and trim, as no constraints were given.

2.2.4. Mesh generation

Fig. 7 shows the volume mesh of this CFD analysis. The built-in automated mesher of Star-CCM + software was used to generate the

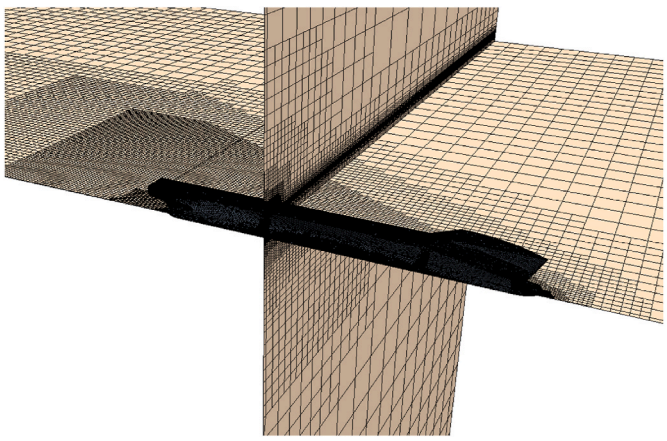

Fig. 7. Volume mesh used for the KCS model simulations.

trimmed hexahedral-dominant finite element mesh. Further near-wall mesh refinements were applied using prism layer meshes on the critical regions such as the free surface, the bulbous bow, the stern, and the rough boundaries regions. For these simulations, the wall y^+ values were kept between 30 and 300 and higher than k^+ values, as recommended by (Siemens, 2020). All the simulations used the same mesh regardless of the hull roughness scenarios.

2.3. Verification and validation

2.3.1. Verification

The verification procedure of the present study was carried out to assess the spatial uncertainty of the simulations. Richardson's Grid Convergence Index (GCI) method, (Richardson, 1911), was adopted as below. According to (Celik et al., 2008), the final expression for the fine-grid convergence index is defined as in equation (9):

$$GCI_{fine}^{21} = \frac{1.25 e_a^{21}}{r_{21}^{p_a} - 1} \tag{9}$$

where, e_a^{21} is the approximate relative error of the key variables, φ_k, i.e., total resistance coefficient, C_T, obtained by equation (10):

$$e_a^{21} = \left| \frac{\varphi_1 - \varphi_2}{\varphi_1} \right| \tag{10}$$

r_{21} is the refinement factor given by $r_{21} = \sqrt[3]{N_1/N_2}$, where N_1 and N_2 are the fine and medium cell numbers, respectively. And the apparent order of the method, p_a, is determined by solving equations (11) and (12) iteratively:

$$p_a = \frac{1}{\ln(r_{21})} \left| \ln \left| \frac{\varepsilon_{32}}{\varepsilon_{21}} \right| + q(p_a) \right| \tag{11}$$

$$q(p_a) = \ln \left(\frac{r_{21}^{p_a} - s}{r_{32}^{p_a} - s} \right) \tag{12}$$

where $s = sign\left(\frac{\varepsilon_{32}}{\varepsilon_{21}}\right)$, $\varepsilon_{32} = \varphi_3 - \varphi_2$, $\varepsilon_{21} = \varphi_2 - \varphi_1$ and r_{32} is the refinement factor given by $r_{32} = \sqrt[3]{N_2/N_3}$, where N_3 is the coarse cell number.

The extrapolated value of the key variables is calculated by equation (13):

$$\varphi_{ext}^{21} = \frac{r_{21}\varphi_1 - \varphi_2}{r_{21} - 1} \tag{13}$$

The extrapolated relative error, e_{ext}^{21}, is obtained by equation (14):

$$e_{ext}^{21} = \left| \frac{\varphi_{ext}^{21} - \varphi_1}{\varphi_{ext}^{21}} \right| \quad (14)$$

Table 3 depicts the required parameters for the calculation of the spatial uncertainty of the simulation. A grid convergence index, GCI_{fine}^{21}, of 0.20% was estimated for the fine-grid simulations conducted in the smooth surface condition with the inlet speed of 1.426 m/s ($R_n = 3.7 \cdot 10^6$), when using ten iterations every time step of 0.01 *s*.

In comparison to the simulation in (Song et al., 2020b), the number of cells of the present study has registered an 11% increase, from 1,306, 433 to 1,462,274. The increase is due to the extra mesh refinements added at strategic locations of the hull, where the transition from smooth to rough conditions is expected. The estimated GCI value of 0.20% indicates the accuracy of the resistance prediction of the effect of the heterogeneous distribution of hull roughness on the KCS model.

2.3.2. Validation

Table 4 compares the total resistance coefficient, C_T, values predicted from the present CFD simulations of the KCS model and the results of (Song et al., 2021a). The comparison was conducted for total resistance coefficients of the full smooth and full rough surface conditions (i.e., C_{T_S} and C_{T_R}) conducted at the design speed of KCS (24 knots) with the corresponding Froude number of 0.26.

In Table 4, the resistance coefficients values from the present CFD simulations were compared against the experimental values read graphically from (Song et al., 2021a). As said in paragraph 2.2.3., the present CFD resistance coefficients were calculated using the same WSA of (Song et al., 2021a). The table above shows that the differences are acceptable, especially given the uncertainties evaluated in the experimental resistance coefficients (Song et al., 2021a). In other words, the total resistance coefficient values, C_T, predicted from the present CFD simulations agrees well with experimental C_T values. Therefore, this agreement confirms that the modified wall-function approach adopted in this study can accurately predict the increased skin friction due to the heterogeneous surface roughness.

3. Results

3.1. Effect of heterogeneous roughness on ship resistance

The conventional simplification of treating hull surfaces as uniformly rough may introduce uncertainties in the added resistance prediction. Heterogeneous hull roughness affects the ship performance in a complicated, non-linear way as it influences both frictional and wave-making resistance (Schultz and Flack, 2007). Furthermore, the location of the increased roughness on the hull has a profound influence on its overall effect on ship resistance (Song et al., 2021b; Kim et al., 2022). Therefore, this study investigated the effect of the heterogeneous distribution of hull roughness on ship resistance. This section discusses and compares the results of the towing tests conducted in CFD on the KCS model in heterogeneous hull roughness conditions with the homogeneous fully smooth and fully rough cases. As reported above in Table 1, the simulations were carried out at a towing speed of 1.426 m/s, Froude number $Fn = 0.26$, and Reynolds number $Re_L = 3.74 \times 10^6$, which correspond to the full-scale design speed of KCS (24 knots) and $Re_L = 2.43 \times 10^9$. The total ship resistance coefficient, C_T, can be decomposed into the frictional, C_F, and the residuary, C_R resistance coefficients, as given by equation (15):

$$C_T = C_F + C_R \quad (15)$$

The C_F and C_R terms were obtained by separating the shear (i.e., frictional resistance) and the pressure (i.e., residual resistance) force components. The residuary resistance can be further decomposed into the viscous pressure resistance, C_{VP}, and the wave-making resistance coefficient, C_W, as in equation (17):

$$C_R = C_{VP} + C_W \quad (16)$$

The total resistance coefficient, C_T, is defined in equation (16) as a function of the total drag, R_T, the dynamic pressure, and the hull wetted surface area, S:

$$C_T = \frac{R_T}{\frac{1}{2}\rho S V^2} \quad (17)$$

in which ρ is the water density and V is the towing speed (i.e., the inlet velocity). Similar formulations can define the other dimensionless resistance coefficients. The total added resistance coefficient (or roughness allowance, ΔC_T) is the variation in the total resistance coefficient between the rough, C_{T_R}, and smooth, C_{T_S}, conditions, equation (18):

$$\Delta C_T = C_{T_R} - C_{T_S} \quad (18)$$

Fig. 8 and Table 5 compare the resistance coefficients of the KCS hull in heterogeneous roughness configurations calculated using the WSA of the present simulations. Different ΔC_T values were found across the fore-rough conditions (*Bulbous Bow*, *Fore Hull*), the midship-rough conditions (*Midship*, *Flat Bottom*), and the aft-rough conditions (*Aft Hull*, *Stern*) due to the different local increased hull roughness and hence locally increased skin friction of the hull. It would be expected that larger rough/smooth wetted surface area ratios would correspond to more significant resistance coefficients.

On the other hand, the present CFD simulations discredited the linear assumption that the larger the area, the more significant the impact. Therefore, e.g., the *Bulbous Bow* case accounts for a smaller rough/smooth wetted surface area ratio than the Stern configuration, but its corresponding added resistance is more significant. As shown in Tables 5 and 6, the *Bulbous Bow* rough/smooth wetted surface area ratio is 2.57%, and the added resistance coefficient is $9.68 \cdot 10^{-5}$ while for the *Stern* case, these parameters are 8.14% and $6/01 \cdot 10^{-5}$, respectively. In other words, the results of this study showed that the position of the selected area of the hull with increased surface roughness strongly affects its impact on the ship hydrodynamics.

Table 6 highlights the non-proportional impact of increased roughness of the heterogeneous configurations. To weighting the effect of

Table 3
Parameters used for the discretisation error for the spatial convergence study, key variable: C_T.

	KCS model simulation
N_1	410,448
N_2	764,370
N_3	1,462,274
r_{21}	1.24
r_{32}	1.23
φ_1	$4.365 \cdot 10^{-3}$
φ_2	$4.232 \cdot 10^{-3}$
φ_3	$4.226 \cdot 10^{-3}$
ε_{32}	$-5.83 \cdot 10^{-6}$
ε_{21}	$-1.33 \cdot 10^{-4}$
s	1
e_a^{21}	3.04%
q	0.13
p_a	13.85
φ_{ext}^{21}	$4.372 \cdot 10^{-3}$
e_{ext}^{21}	−0.16%
GCI_{fine}^{21}	0.20%

Table 4
Parameters used for the validation of the present CFD simulations.

	Present CFD	EFD (Song et al., 2021a)	Difference
C_{T_S}	$4.366 \cdot 10^{-03}$	$4.185 \cdot 10^{-3}$	− 0.39%
C_{T_R}	$6.034 \cdot 10^{-03}$	$5.820 \cdot 10^{-3}$	0.33%

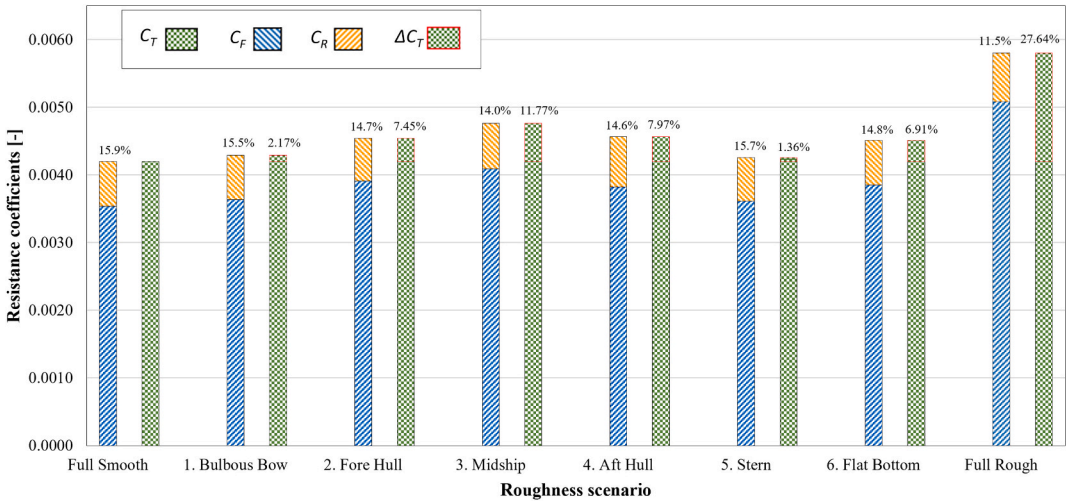

Fig. 8. Percentage bar diagram of the resistance coefficients in different hull roughness conditions.

Table 5
Resistance coefficients for the KCS model simulations in different hull roughness conditions.

Roughness scenario	Total resistance coefficient C_T	Frictional resistance coefficient C_F		Residuary resistance coefficient C_R		Added resistance coefficient ΔC_T	
Full smooth	$4.37{\cdot}10^{-3}$	$3.67{\cdot}10^{-3}$	84.1%	$6.93{\cdot}10^{-4}$	15.9%	0.00	0.00%
1. Bulbous Bow	$4.46{\cdot}10^{-3}$	$3.78{\cdot}10^{-3}$	82.3%	$6.87{\cdot}10^{-4}$	15.5%	$9.68{\cdot}10^{-5}$	2.17%
2. Fore Hull	$4.72{\cdot}10^{-3}$	$4.06{\cdot}10^{-3}$	77.9%	$6.57{\cdot}10^{-4}$	14.7%	$3.52{\cdot}10^{-4}$	7.45%
3. Midship	$4.95{\cdot}10^{-3}$	$4.25{\cdot}10^{-3}$	74.2%	$7.00{\cdot}10^{-4}$	14.0%	$5.82{\cdot}10^{-4}$	11.77%
4. Aft Hull	$4.74{\cdot}10^{-3}$	$3.97{\cdot}10^{-3}$	77.4%	$7.73{\cdot}10^{-4}$	14.6%	$3.78{\cdot}10^{-4}$	7.97%
5. Stern	$4.43{\cdot}10^{-3}$	$3.75{\cdot}10^{-3}$	83.0%	$6.72{\cdot}10^{-4}$	15.7%	$6.01{\cdot}10^{-5}$	1.36%
6. Flat Bottom	$4.69{\cdot}10^{-3}$	$4.00{\cdot}10^{-3}$	78.3%	$6.90{\cdot}10^{-4}$	14.8%	$3.24{\cdot}10^{-4}$	6.91%
Full Rough	$6.03{\cdot}10^{-3}$	$5.28{\cdot}10^{-3}$	60.9%	$7.51{\cdot}10^{-4}$	11.5%	$1.67{\cdot}10^{-5}$	27.64%

Table 6
Roughness impact factors and wetted surface area ratios of the roughness scenario tested.

Roughness scenario	Rough wetted surface area % WSA_R	Added resistance coefficient % ΔC_T	Added effective power % ΔP_e	Roughness Impact Factor RIF
Full Smooth	0	0	0	0
1. Bulbous Bow	2.57	2.17	2.22	2.26
2. Fore Hull	17.68	7.45	8.05	1.19
3. Midship	29.49	11.77	13.34	1.18
4. Aft Hull	19.12	7.97	8.66	1.19
5. Stern	8.14	1.36	1.38	0.44
6. Flat Bottom	22.91	6.91	7.42	0.85
Full Rough	100	27.64	38.20	1

increased heterogeneous hull roughness on added resistance, a so-called "Roughness Impact Factor", *RIF*, has been defined as in equation (19):

$$RIF = \frac{(\Delta C_T)_i}{(WSA_{Rough})_i} \Big/ \frac{(\Delta C_T)_{Full\ Rough}}{WSA_{Total}} \tag{19}$$

In which $(\Delta C_T)_i$ and $(WSA_{Rough})_i$ are, respectively, the total added resistance and the rough wetted surface area of the i-th heterogeneous hull roughness scenario. $(\Delta C_T)_{Full\ Rough}$ is the added resistance of the full rough hull surface condition, and WSA_{Total} is the total wetted surface area of the hull. Evidently, the roughness impact factor *RIF* is unitary for the *Full Rough* scenario. In other words, *RIF* correlates the added resistance coefficient to the rough wetted surface area of any given roughness condition.

It can be noted that while being the smallest area with increased hull roughness, the *Bulbous Bow* scenario has the most significant impact on ship resistance (impact factor of 2.26) of all the scenarios. The *Fore Hull/ Aft Hull* cases have the second-largest effect (impact factor of 1.19). On the other hand, despite being the largest rough wetted surface area tested, the *Midship* configuration only gives an impact factor of 1.18. Similarly, the *Stern,* and *Flat Bottom* configurations showed the lowest impact factors of the heterogeneous scenarios tested. For these configurations, *RIF* is lower than unity (0.44, 0.85, respectively). Similarly to (Tezdogan et al., 2015), the effective power penalty for the KCS model, ΔP_E, was estimated as in equation (20):

$$\%\Delta P_E = \frac{\Delta C_T}{C_{TS}} 100 \tag{20}$$

The impact of the different roughness scenarios on the effective power is presented in Table 6. Once again, the *Bulbous Bow* rough case, regardless of the limited rough wetted area (2.57%), has a significant impact on hydrodynamic performances. Hence, the added effective

power of the KCS model with a rough bulbous bow is 2.22%. Therefore, assuming a similar outcome for full-scale conditions, it seems reasonable to tackle the increased hull roughness on the bulbous bow region promptly.

3.2. The rationale behind the effect of heterogeneous roughness

The effect of hull roughness on ship resistance is closely related to the heterogeneous distribution of the increased roughness. Locally increased roughness affects the local skin friction coefficients, the Roughness Reynolds number values (k^+) and the boundary layer characteristics. A discussion and comparison of the local skin friction, the roughness Reynolds number and the boundary layer of the KCS hull with heterogeneous hull roughness scenarios are presented.

Fig. 9 compares the local skin friction coefficients, C_f, on the KCS hull in heterogeneous hull roughness conditions with the homogeneous full smooth and full rough cases (scalar field distribution on the hull surfaces limited to $C_f = 0.01$). The local skin friction coefficients, C_f, were obtained as in equation (21):

$$C_f = \frac{\tau_w}{0.5\,\rho\,V^2} \tag{21}$$

Where τ_w is the wall shear stress, ρ is the water density, and V is the towing speed (i.e., the inlet velocity). The *Bulbous Bow* and *Fore Hull* roughness conditions in Figs. 9–1 and Figs. 9–2 show similar C_f distributions as that of the *Full Rough* condition. The most significant increases in the local C_f values were observed for the upstream regions of the *Midship* configuration. In this case, the effect of the heterogeneous increase of hull roughness is dramatic, as shown in Figs. 9–3. On the other hand, the *Aft Hull*, *Stern,* and *Flat Bottom* scenarios (Figs. 9–4,5,6) are less impactful on the skin friction coefficient distribution. Hence, C_f distributions are more similar to the *Full Smooth* homogeneous condition than to the *Full Rough*.

The observation in Figs. 9 and 10 on the local skin friction coefficients, C_f, and the roughness Reynolds numbers, k^+, are strictly related to the previous findings shown in Tables 5 and 6. It is well-known that the wall shear stress, τ_w, is more significant in the bow region of ship hulls due to the active transition behaviours, and it decreases as the flow develops along the hull. Furthermore, the flow is less de-accelerated in the bow area and has a less developed boundary layer, resulting in a thinner boundary layer. Hence, the roughness height will occupy a larger fraction of the boundary layer and result in a higher skin friction coefficient. As the wall shear stress, τ_w, increases, it results in larger local skin friction coefficients and roughness Reynolds numbers in the bow regions. Accordingly, the roughness effect in the bow regions becomes more critical than in the stern areas.

It may be demonstrated that the higher the wall-shear stress, the lower the probability of that hull region experiencing severely increased roughness. Although this phenomenon is not yet well documented in the literature, it is known that higher stress on "Foul Release Coatings" implies minor biofouling accumulation. On the other hand, for vessels coated with "Self-Polishing Coatings", higher stress implies that these coatings are worn off faster and, when wholly depleted, would increase bioaccumulation. Nevertheless, it is well demonstrated that fouling organisms attach more easily to stationary vessels as neither "Self-Polishing Coatings" nor "Foul Release coatings" are effective for stationary vessels. It is evident that the parameter most influencing the hull roughness for ships that spend longer time stationary would not be the wall-shear stress. For stationary ships, other parameters such as light exposure would perhaps lead to a more severe heterogeneous distribution of hull roughness.

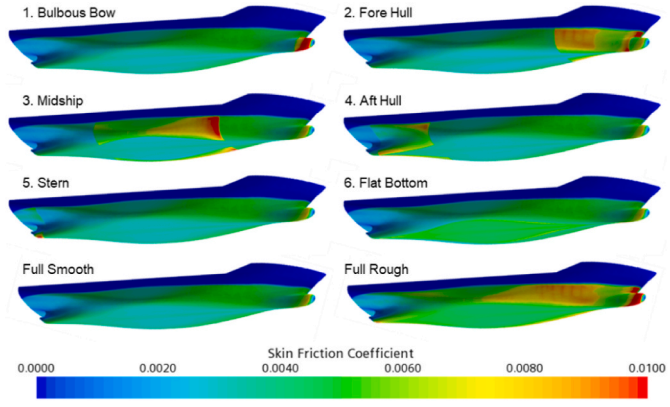

Fig. 9. Skin friction coefficients (C_f) on the KCS hull in different hull roughness conditions ($Fn = 0.26$).

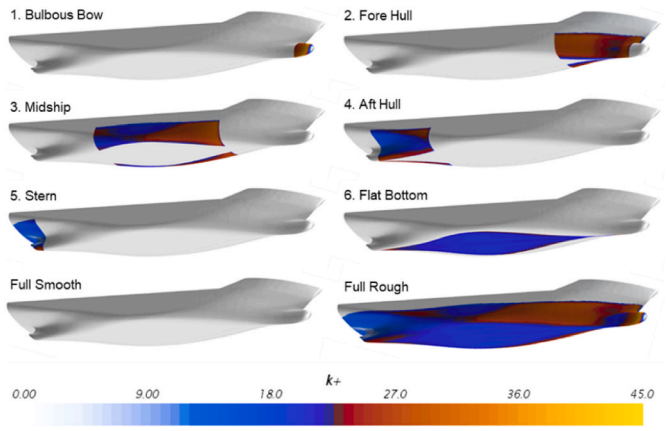

Fig. 10. Roughness Reynolds number (k^+) on the KCS hull in different hull roughness conditions ($Fn = 0.26$).

Fig. 10 shows the distributions of the roughness Reynolds number, k^+, on the KCS hull in heterogeneous hull roughness conditions (scalar field distribution on the hull surfaces limited to $k^+ = 45.0$). The roughness Reynolds numbers were obtained as in equation (6). As shown in equation (8), the fully rough regime is reached when k^+ value is higher than 25. The distributions of k^+ on the heterogeneous rough surfaces is similar to the bow regions of the homogeneous *Full Rough* case. Accordingly, configurations 1, 2 and 3 show larger k^+ values than the scenarios 4, 5 and 6 due to the observed roughness effect.

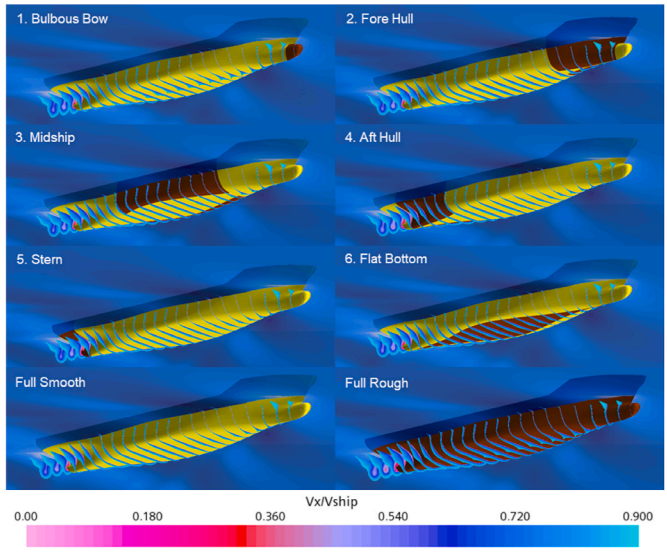

Fig. 11. Boundary layer on the KCS hull in different hull roughness conditions at the test speed ($Fn = 0.26$).

The Full Rough scenario shows a thicker boundary layer than the Full Smooth condition for the homogeneous cases. Fig. 11 shows another notable feature of the effect of heterogeneous hull roughness on the ship resistance, i.e., the boundary layer contours on the KCS hull in different hull roughness conditions. The boundary layer is represented by portions of transversal planes limited to the axial velocity, $V_x/\ V_{ship} = 0.9$. The roughness increase affects the boundary layer thickness around the hull, which is defined as the distance between the wall and the point where the velocity magnitude of the flow parallel to the wall, V_x, reaches the proportion of 0.99 of the free-stream velocity, V_{ship}, i.e., $V_x = 0.99\ V_{ship}$. As shown in Fig. 11, the velocity in the turbulent boundary layer decreases with roughness on the hull surface. This velocity decrease manifests itself as an increase in the frictional resistance Figs. 9 and 10. On the other hand, the increase of roughness leads to an increase in turbulence and turbulent kinetic energy, which means that the turbulent stress and wall shear stress increase. The present findings are in agreement with previous studies of other researches (Schultz and Flack, 2005, 2007; Demirel et al., 2017b; Song et al., 2019; Song et al., 2021b). The Full Rough scenario shows a thicker boundary layer than the Full Smooth condition for the homogeneous cases.

Furthermore, the differences between *Full Rough* and *Full Smooth* configurations become apparent in the bow regions where the increased roughness causes a thicker boundary layer, peak-shaped on the symmetry plane. Notably, the boundary layer contours shown in Fig. 11 present a spike at the centre plane, particularly evident in the Bulbous Bow and Full Rough cases. Such a recognisable shape is due to the implementation of symmetry conditions at the symmetry plane, as discussed in other research studies such as (Demirel et al., 2017b) and (Song et al., 2020a). Hence, the rationale behind the significant Roughness Impact Factor of the Bulbous Bow region may lie in its extensive influence on the boundary layer characteristics. Interestingly, the boundary layer of the *Bulbous Bow* case (Figs. 11–1) is similar to that of the *Full Rough* condition. While, despite a similar thickness of the boundary layer, the *Fore Hull* case shows a much less evident pointy shape (Figs. 11–2). On the other hand, as shown in Figs. 11–3,4,5,6, the boundary layer thickness around the hull showed almost no differences compared to that of the *Full Smooth* case.

One may notice that the understanding of the roughness effect on various hydrodynamic aspects, such as the boundary layer thickness, is still limited. Therefore, additional analyses could be carried out, including broad variations of speeds, scales, and hull forms. Further investigation could exclude the free surface in the viscous pressure resistance, C_{VP}, term to illustrate that the viscous pressure resistance ratio changes (akin to the form factor). Hence, an expected result would be that roughness in the stern area would have the highest ratio of C_{VP}.

4. Conclusions

An investigation on the effect of heterogeneous hull roughness on ship resistance components and characteristics of the flow around the hull was carried out. URANS-based CFD simulations were carried out on the well-known KCS hull model in different hull roughness conditions. A modified wall-function approach was adopted to implement the roughness characteristics of the surfaces in the CFD model. The different scenarios studied were intended to assess the roughness effect of different parts of the hull on the ship hydrodynamics. The observations on the effects of heterogeneous hull roughness were correlated with the rough wetted surface areas, the distributions of the local skin friction coefficients, the roughness Reynolds number values, and the boundary layer characteristics. Furthermore, comparisons with the homogeneous full rough-smooth cases were presented.

The CFD towing tests showed that the rough regions tested (*Bulbous Bow*, *Fore Hull*, *Midship*, *Aft Hull*, *Stern* and *Flat Bottom*) had a different impact on the ship resistance due to their position on the hull. A *roughness impact factor*, *RIF*, was defined to predict this impact. The added resistance observed for the fore-rough regions was proportionately greater than for the aft-rough regions with the same surface roughness conditions. In other words, the roughness conditions of the fore regions proportionally affect the ship hydrodynamics more than the aft regions. The present study supported similar observations of other researchers (Schultz and Flack, 2005, 2007; Demirel et al., 2017b; Song et al., 2019; Song et al., 2021b).

The numerical investigation presented in this study provides valuable results from a practical point of view. The roughness impact of different hull regions has been investigated, adopting a widely accepted and validated CFD approach. Interestingly, the present findings showed that among all the scenarios, the rough Bulbous Bow condition presents the greatest roughness impact factor ($RIF = 2.26$), despite the smallest percentage of rough wetted surface area. Thus, the rough bulbous bow scenario led to proportionately greater added resistance than other rough regions of the hull. Therefore, partial hull cleaning of the bow part would be more beneficial than cleaning an equal surface area in another part of the wetted surface. On the other hand, the rough *Stern* case presents the smaller roughness impact factor ($RIF = 0.44$), suggesting the surface conditions of the aft regions of the hull have a minor impact on ship resistance. Naval architects, ship owners, and operators could benefit from this study's insight and target limited-time maintenance on the fore-hull regions affecting the ship resistance the most. When complete maintenance on the entire hull is not feasible, it could be worth cleaning the fore hull parts first.

This study provided several significant findings, including the definition of the roughness impact factor to assess the effect of heterogeneous hull roughness on ship resistance. Intuitively, the hull roughness causes substantial increases in the frictional resistance regardless of the heterogeneous configurations. However, it is worth considering that hull areas are characterised by specific wall shear stress and heterogeneous surface roughness distributions affecting the ship resistance in different ways. Areas of the hull with low wall shear stress would likely be heavily fouled and vice-versa. A rougher surface would characterise the most degraded areas. Detailed correlations between heterogeneous hull roughness distributions and the occurrence probability on specific parts of the hull could be further analysed.

The authors understand that for the propulsion of ships, the hull surface roughness will significantly affect ship resistance as the wake can be affected significantly. Therefore, the numbers presented in the present study are not the full story leading to assessing fuel consumption effects. Future studies could compare the numerical results presented in this study with measurements obtained from EFD tow tests and investigate self-propulsion simulations. Novel heterogeneous hull roughness configurations, in model and full scale, and their effect on ship resistance could be investigated. Further investigations could also exploit the relationship between hull roughness distribution and vortex development, pressure distribution, turbulence kinetic energy, vorticity, flow recovery, and wake development.

CRediT authorship contribution statement

Roberto Ravenna: Conceptualization, Methodology, Formal analysis, Investigation, Data curation, Comparison, Writing – original draft, Visualization. **Soonseok Song:** Conceptualization, Methodology, Formal analysis, Investigation, Data curation, Comparison, Writing – review & editing. **Weichao Shi:** Supervision, Conceptualization, Methodology, Writing – review & editing. **Tonio Sant:** Funding acquisition, Project administration, Writing – review & editing. **Claire De Marco Muscat-Fenech:** Funding acquisition, Project administration, Writing – review & editing. **Tahsin Tezdogan:** Conceptualization, Methodology, Resources, Writing – review & editing. **Yigit Kemal Demirel:** Conceptualization, Methodology, Resources, Writing – review & editing.

Declaration of competing interest

The authors declare that they have no known competing financial interests or personal relationships that could have appeared to influence the work reported in this paper.

Acknowledgements

This paper is based on the study presented at the 2nd International Congress on Ship and Marine Technology (GMO-SHIPMAR 2021) organised by the Turkish Chamber of Naval Architects and Marine Engineers (GMO), which was held on September 16–18, 2021, at Yildiz Technical University, in Istanbul, Turkey. The authors gratefully acknowledge that the research presented in this paper was carried out as part of the EU funded H2020 project, VENTuRE (grant no. 856887, https://h2020venture.eu/). This work was also supported by Inha University Research Grant. It should be noted that the results presented in this study were obtained using the ARCHIE-WeSt High-Performance Computer (www.archie-west.ac.uk) based at the University of Strathclyde.

References

Atlar, M., et al., 2018. A rational approach to predicting the effect of fouling control systems on "In-service" ship performance. GMO J. Ship Mar. Technol. 213. https://strathprints.strath.ac.uk/66052/.

Candries, M., 2001. Drag, Boundary-Layer and Roughness Characteristics of Marine Surfaces Coated with Antifoulings. University of Newcastle. Available at: https://www.researchgate.net/publication/34521559.

Celik, I., et al., 2008. Procedure for estimation and reporting of uncertainty due to discretization in CFD applications. J. Fluid Eng. 130 (–2), 078001 https://doi.org/10.1115/1.2960953.

Demirel, Y.K., 2015. Modelling the Roughness Effects of Marine Coatings and Biofouling on Ship Frictional Resistance. University of Strathclyde. Available at: http://digitool.lib.strath.ac.uk:80/R/?func=dbin-jump-full&object_id=26005.

Demirel, Y.K., et al., 2017a. Effect of barnacle fouling on ship resistance and powering. Biofouling 33 (10), 819–834. https://doi.org/10.1080/08927014.2017.1373279.

Demirel, Y.K., et al., 2019. Practical added resistance diagrams to predict fouling impact on ship performance. Ocean Eng. 186 (June), 106112 https://doi.org/10.1016/j.oceaneng.2019.106112.

Demirel, Y.K., Turan, O., Incecik, A., 2017b. Predicting the effect of biofouling on ship resistance using CFD. Appl. Ocean Res. 62, 100–118. https://doi.org/10.1016/j.apor.2016.12.003.

Farkas, A., et al., 2020. Impact of biofilm on the ship propulsion characteristics and the speed reduction. Ocean Eng. 199, 107033 https://doi.org/10.1016/j.oceaneng.2020.107033.

Farkas, A., Degiuli, N., Martić, I., 2018. Towards the prediction of the effect of biofilm on the ship resistance using CFD. Ocean Eng. 167 (August), 169–186. https://doi.org/10.1016/j.oceaneng.2018.08.055.

Ferziger, J.H., Perić, M., Street, R.L., 2020. Computational Methods for Fluid Dynamics, Computational Methods for Fluid Dynamics. Springer International Publishing. https://doi.org/10.1007/978-3-319-99693-6.

Flack, K.A., Schultz, M.P., 2010. Review of hydraulic roughness scales in the fully rough regime. J. Fluids Eng. Transact. ASME. https://doi.org/10.1115/1.4001492, 0412031–04120310.

Granville, P.S., 1958. The frictional resistance and turbulent boundary layer of rough surfaces. J. Ship Res. 2 (4), 52–74. https://doi.org/10.5957/jsr.1958.2.4.52.

Granville, P.S., 1978. Similarity-law Characterization Methods for Arbitrary Hydrodynamic Roughnesses. David W Taylor Naval Ship Research and Development Center Bethesda Md Ship Performance Dept, Bethesda: Rockville, MD, USA. https://apps.dtic.mil/sti/citations/ADA053563.

Haslbeck, E.G., et al., 1992. Microbial biofilm effects on drag - lab and field. In: Proceedings of the Ship Production Symposium. The National Shipbuilding Research Program, New Orleans, Louisiana. https://ia601309.us.archive.org/35/items/DTIC_ADP023028.

ITTC, 2011. Recommended Procedures and Guidelines - Practical Guidelines for Ship CFD Applications. ITTC. https://www.ittc.info/media/1357/75-03-02-03.

KCS Geometry and Conditions, 2008. SIMMAN 2008, FORCE Technology. Available at: http://www.simman2008.dk/KCS/kcs_geometry.htm.

Kim, K., Leer-Andersen, M., Werner, S., 2022. A study on the effect of hull surface treatments ON SHIP performances. In: The 9th Conference on Computational Methods in Marine Engineering (Marine 2021), 1. https://doi.org/10.2218/MARINE2021.6785, 1.

Kim, W.J., Van, S.H., Kim, D.H., 2001. Measurement of flows around modern commercial ship models. Exp. Fluid 31 (5), 567–578. https://doi.org/10.1007/s003480100332.

Larsson, L., Stern, F., Visonneau, M., 2013. CFD in ship hydrodynamics - results of the Gothenburg 2010 workshop. In: Computational Methods in Applied Sciences. Springer Netherland, pp. 237–259. https://doi.org/10.1007/978-94-007-6143-8_14.

Menter, F.R., 1994. Two-equation eddy-viscosity turbulence models for engineering applications. AIA A J. 32 (8) https://doi.org/10.2514/3.12149.

Oliveira, D., Larsson, A.I., Granhag, L., 2018. Effect of ship hull form on the resistance penalty from biofouling. Biofouling 34 (3), 262–272. https://doi.org/10.1080/08927014.2018.1434157.

Östman, A., Koushan, K., Savio, L., 2019. Study on additional ship resistance due to roughness using CFD. J. Ship Marine Technol. 216. Available at: http://www.gmoshipmar.org/,Dergianasayfası http://www.gmoshipmar.org/.

Richardson, L.F., 1911. IX. The approximate arithmetical solution by finite differences of physical problems involving differential equations, with an application to the stresses in a masonry dam. Philos. Trans. R. Soc. Lond. - Ser. A Contain. Pap. a Math. or Phys. Character 210 (459–470), 307–357. https://doi.org/10.1098/RSTA.1911.0009.

Schultz, M.P., 2002. The relationship between frictional resistance and roughness for surfaces smoothed by sanding. J. Fluids Eng. Transact. ASME 124 (2), 492–499. https://doi.org/10.1115/1.1459073.

Schultz, M.P., 2004a. Frictional resistance of antifouling coating systems. J. Fluids Eng. Transact. ASME 126 (6), 1039–1047. https://doi.org/10.1115/1.1845552.

Schultz, M.P., 2004b. Frictional resistance of antifouling coating systems. J. Fluid Eng. 126 (6), 1039. https://doi.org/10.1115/1.1845552.

Schultz, M.P., 2007. Effects of coating roughness and biofouling on ship resistance and powering. Biofouling 23 (5), 331–341. https://doi.org/10.1080/08927010701461974.

Schultz, M.P., Flack, K.A., 2005. Outer layer similarity in fully rough turbulent boundary layers. Exp. Fluid 38 (3), 328–340. https://doi.org/10.1007/s00348-004-0903-2.

Schultz, M.P., Flack, K.A., 2007. The rough-wall turbulent boundary layer from the hydraulically smooth to the fully rough regime. J. Fluid Mech. 580, 381–405. https://doi.org/10.1017/S0022112007005502.

Schultz, M.P., Swain, G.W., 2000. The effect of biofilms on turbulent boundary layers. J. Fluid Eng. 121 (1), 44. https://doi.org/10.1115/1.2822009.

Shapiro, T., 2004. *The Effect of surface Roughness on hydrodynamic Drag and turbulence*. US naval academy annapolis. Available at: https://apps.dtic.mil/dtic/tr/fulltext/u2/a424978.pdf.

Song, S., Demirel, Y.K., De Marco Muscat-Fenech, C., et al., 2020a. Fouling effect on the resistance of different ship types. Ocean Eng. 216, 107736 https://doi.org/10.1016/j.oceaneng.2020.107736.

Song, S., Demirel, Y.K., De Marco Muscat-Fenech, C., et al., 2020b. Fouling effect on the resistance of different ship types. Ocean Eng. 216 (June), 107736 https://doi.org/10.1016/j.oceaneng.2020.107736.

Song, S., Demirel, Y.K., Atlar, M., et al., 2020c. Validation of the CFD approach for modelling roughness effect on ship resistance. Ocean Eng. 200 (February), 107029 https://doi.org/10.1016/j.oceaneng.2020.107029.

Siemens, 2020. Simcenter STAR-CCM+ User Guide. Version 15.06. Siemens. https://www.plm.automation.siemens.com/global/pl/products/simcenter/STAR-CCM.html.

Song, S., Dai, S., Demirel, Y.K., Atlar, M., et al., 2021a. Experimental and theoretical study of the effect of hull roughness on ship resistance. J. Ship Res. 65 (1), 62–71. https://doi.org/10.5957/josr.07190040.

Song, S., Ravenna, R., Dai, S., De Marco Muscat-Fenech, C., et al., 2021b. Experimental investigation on the effect of heterogeneous hull roughness on ship resistance. Ocean Eng. 223 https://doi.org/10.1016/j.oceaneng.2021.108590.

Song, S., Ravenna, R., Dai, S., De marco Muscat-Fenech, C., et al., 2021c. Experimental Investigation on the Effect of Heterogeneous Hull Roughness on Ship Resistance. https://doi.org/10.1016/j.oceaneng.2021.108590.

Song, S., Demirel, Y.K., De Marco Muscat-Fenech, C., Sant, T., et al., 2021d. Investigating the effect of heterogeneous hull roughness on ship resistance using CFD. J. Mar. Sci. Eng. 9 (202) https://doi.org/10.3390/jmse9020202.

Song, S., Demirel, Y.K., Atlar, M., 2019. An investigation into the effect of biofouling on the ship hydrodynamic characteristics using CFD. Ocean Eng. 175 (January), 122–137. https://doi.org/10.1016/j.oceaneng.2019.01.056.

Song, S., Demirel, Y.K., Atlar, M., 2020d. Penalty of hull and propeller fouling on ship self-propulsion performance. Appl. Ocean Res. 94 (July 2019), 102006 https://doi.org/10.1016/j.apor.2019.102006.

Stern, F., et al., 2015. Recent progress in CFD for naval architecture and ocean engineering. J. Hydrodyn. 1–23. https://doi.org/10.1016/S1001-6058(15)60452-8.

Terziev, M., Tezdogan, T., Incecik, A., 2020. Application of eddy-viscosity turbulence models to problems in ship hydrodynamics. Ships Offshore Struct. 15 (5), 511–534. https://doi.org/10.1080/17445302.2019.1661625.

Tezdogan, T., et al., 2015. Full-scale unsteady RANS CFD simulations of ship behaviour and performance in head seas due to slow steaming. Ocean Eng. 97, 186–206. https://doi.org/10.1016/j.oceaneng.2015.01.011.

Tezdogan, T., Demirel, Y.K., 2014. An overview of marine corrosion protection with a focus on cathodic protection and coatings. Brodogradnja/Shipbuilding 65 (2), 49–59. https://strathprints.strath.ac.uk/51802/1.

Townsin, R.L., 2003. The ship hull fouling penalty. Biofouling 19 (Suppl. 1), 9–15. https://doi.org/10.1080/0892701031000088535.

Vargas, A., Shan, H., Holm, E., 2019. Using CFD to predict ship resistance due to biofouling, and plan hull maintenance. In: 4th Hull Performance & Insight Conference (HullPIC), pp. 242–254. Gubbio, Italy. http://data.hullpic.info/HullPIC2019.